ISSN (Print) 1226-1750
ISSN (Online) 2233-6656
Journal of Magnetics 23(3), 416-422 (2018) https://doi.org/10.4283/JMAG.2018.23.3.416

Evolution of Residual Magnetic Field of U75V Steel Induced by Uniaxial Tensile Load with Increasing Amplitudes

Meili Fu[1,2], Sheng Bao[1]*, and Shiwei Lin[3]

[1]*Institute of Structural Engineering, Zhejiang University, Hangzhou, 310058, PR China*
[2]*Seazen Holdings Co., Ltd., Shanghai, 200062, PR China*
[3]*School of Civil Engineering, Dalian University of Technology, Dalian, 116000, PR China*

(Received 12 September 2017, Received in final form 16 September 2018, Accepted 18 September 2018)

In order to investigate the residual magnetic field (RMF) variations of initially undemagnetized ferromagnetic materials, tensile tests were conducted on the U75V steel specimens under tensile load with increasing amplitudes. It is found that the fluctuation of the unidimensional RMF reduces with the increase of load in the elastic stage, and remains relatively stable during the plastic stage. An effective way for characterizing deformation stages of the undemagnetized specimen is proposed by analyzing the RMF signals outside the longitudinal axis of the specimen. The two-dimensional vector distribution of the RMF indicates that the specimen tends to be magnetized as a rectangular magnet with an N pole and S pole at two ends with the increase of load. The possible reasons underlying the experimental results are discussed on the basis of the theory of the interaction between dislocation and domain.

Keywords : residual magnetic field, tensile load, deformation stage, rectangular magnet

1. Introduction

Passive magnetic techniques such as metal magnetic memory (MMM) make use of variations in the residual magnetic field (RMF) of a ferromagnetic material under the combined operation of external loads and ambient geomagnetic field [1]. The MMM technique is suitable for many engineering practices due to its advantages of easy-operation, time-saving and simple criteria. It is regarded to be effective in assessing the early damage as well as fully developed defects [2]. Therefore, there has been an increasing interest in the investigation of the RMF of ferromagnetic materials induced by external loads due to that a strong demand from industry for methods to evaluate the state of stress and deformation [3, 4].

The RMF signals include the tangential component, which is parallel to the specimen surface, and the normal component perpendicular to the specimen surface, which are two basic parameters employed for the MMM technique. In previous research, a number of experiments have been conducted to investigate the effects of stress on the RMF variations in many demagnetized ferromagnetic steels [5-7]. These studies showed that the RMF distributions along scanning lines are approximately linear in the elastic deformation stage. In contrast to elastic deformation, plastic deformation creates dislocation, dislocation tangles and even dislocation cellular structures, which make magnetic behavior in the plastic deformation stage more complex. Factors found to impact on the RMF signals have been qualitatively investigated as well, such as the loading type [7, 8]; the chemical compositions of ferromagnetic materials [9]; the initial magnetic state of the specimen [10, 11]; the geometry and dimensions of the specimen [12, 13]; and the loading speed and loading history [14, 15]. Their research demonstrated that these factors can change the magnitude of the RMF, whereas significant influence on its variation trend or the residual magnetic curve's profile has not been found. Previous work were mainly focused on the investigation of the unidimensional RMF variations of demagnetized materials, nevertheless experimental research on the multidimensional RMF distribution characteristics induced by external loads in undemagnetized materials is scarce. In engineering practices, the initial remanent states of ferromagnetic components are non-uniformly distributed,

*Corresponding author: Tel: +86-0571-8820-8728
Fax: +86-0571-8820-8728, e-mail: longtubao@zju.edu.cn

and the demagnetization for these components is time-consuming and even impractical. Therefore, the comprehensive understanding of the multidimensional magnetic field surrounding an undemagnetized ferromagnetic component is quite important. In this paper, tension tests were carried out, and the multidimensional RMF variations of undemagnetized U75V steel specimens at different load levels were investigated. In the meantime, the possible reasons underlying the experimental results were further discussed.

2. Experimental Details

The tested material was U75V steel which is a common material for rail construction in China characterized with high strength, excellent wear and fatigue resistance, and relatively poor welding performance. Its chemical composition and mechanical properties are listed in Table 1 and Table 2, respectively. Tensile specimens of dimensions 200 mm (length) × 30 mm (width) × 4 mm (thickness) were machined into smooth plate according to the Chinese Standard GB/T228-2002, as shown in Fig. 1 by bold lines. A scanning line with a length of 240 mm was drawn on the surface of the specimen, and 150 points at intervals of 20 mm on an area of 180 mm × 280 mm around the specimen were chosen for the RMF measurement. It should be noted that the specimens were not demagnetized before loading.

The tensile tests were carried out by a universal testing equipment with a peak capacity of 200 kN. The RMF signals were monitored by a magnetic magnetometer TSC-1M-4 and a scanning sensor with a lift-off value of 4 mm, whose measurement sensitivity is 1 A/m. In tensile testing, the specimen was first loaded to a preset load and unloaded to 0 KN, and placed on a non-magnetic scanning platform along the south-north axis. Then, the RMF signals ($H_{t,x}$, $H_{n,z}$) along the scanning line and of 150 measurement points ($H_{t,x}$, $H_{t,y}$) were immediately collected. After that, the specimen was loaded again to a higher predetermined load and unloaded, and the above procedure was repeated until the specimen was fractured. The measurement provides three components of the RMF on the specimen surface as shown in Fig. 1.

- $H_{t,x}$—tangential component measured in the direction parallel to the specimen surface along X axis,
- $H_{t,y}$—tangential component measured in the direction parallel to the specimen surface along Y axis,
- $H_{n,z}$—normal component measured in the direction perpendicular to the specimen surface along Z axis.

Table 1. Chemical composition (wt%) of specimen material.

Material	C	Si	Mn	P	S	V
U75V	0.70-0.78	0.50-0.80	0.70-1.05	≤0.03	≤0.03	0.04-0.12

Table 2. Mechanical properties of specimen material.

Material	Elastic modulus, E (GPa)	Yield strength, σ_y (MPa)	Ultimate tensile strength, σ_u (MPa)
U75V	200	650	980

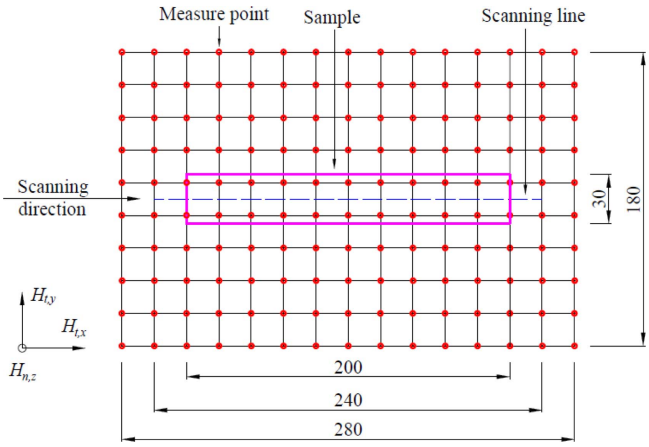

Fig. 1. (Color online) Specimen shape, scanning line and measurement points (unit: mm)

3. Results and Discussions

Figure 2 shows the variations of the $H_{t,x}$ and $H_{n,z}$ components along the scanning line loaded from 0 to 70 kN in the elastic stage. One may observe that the residual magnetic curves change conspicuously at small loads, and then revert to a more gradual rate of change at high loads. The initial $H_{t,x}$ and $H_{n,z}$ at 0 kN fluctuate drastically along the scanning line and resemble sinusoidal waveforms, which suggest the irregular orientation of magnetic domains before loading. One striking event in Fig. 2 is that the change of the magnetic amplitude in three contiguous waveforms as marked between two dashed lines. In Fig. 2(a), the consecutive magnetic amplitudes $\Delta H_{t,x}$ is about 492 A/m at 0 kN. As the load increases to 10 kN, the magnetic fluctuation of $\Delta H_{t,x}$ is reduced to about 379 A/m. The magnetic traces seem to be further compressed at 20 kN, and the corresponding $\Delta H_{t,x}$ is rapidly reduced to about 257 A/m. As the applied load continues to increase by a uniform pace, the fluctuation of the magnetic fields decreases at a more gradual rate and the $H_{t,x}$ curve tends to be a horizontal line. Similar results can also be found in the H_z curve between two dashed lines in Fig. 2(b), the fluctuation of $\Delta H_{n,z}$ is quickly reduced from 600 A/m at 0

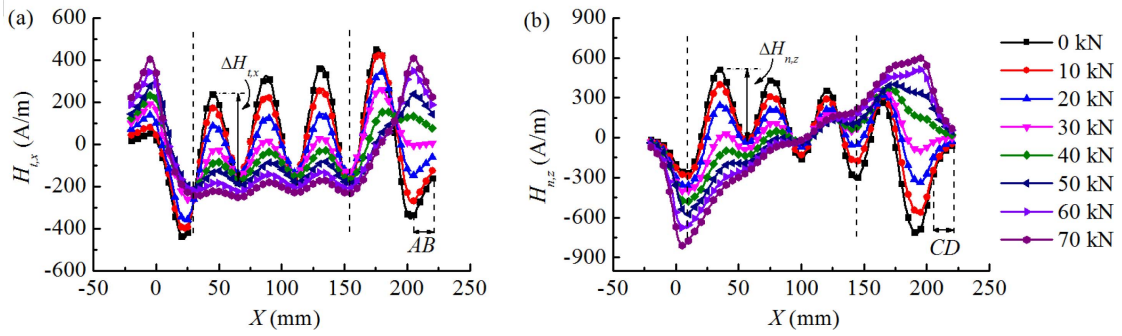

Fig. 2. (Color online) Variation of the RMF components along the scanning line with the increase of load in the elastic stage: (a) tangential component $H_{t,x}$; (b) normal component $H_{n,z}$.

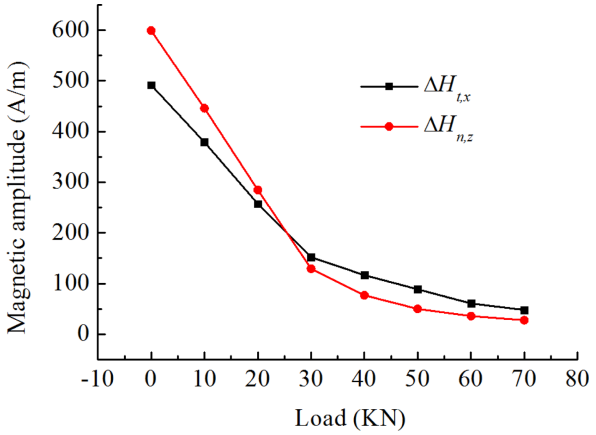

Fig. 3. (Color online) Variations of $\Delta H_{t,x}$ and $\Delta H_{n,z}$ with the increase of load in the elastic stage.

kN to 285 A/m at 20 kN. Thereafter, the $H_{n,z}$ curve rotates counterclockwise with a decreasing rate and evolves into an almost oblique line.

The variations of $\Delta H_{t,x}$ and $\Delta H_{n,z}$ with the increase of load are further displayed in Fig. 3. It can be observed that the stress-induced magnetic behavior of $\Delta H_{t,x}$ resembles that of $\Delta H_{n,z}$. To be specific, with the increase of load from 0 to 30 kN, both $\Delta H_{t,x}$ and $\Delta H_{n,z}$ decrease dramatically from 492 to 152 A/m and from 600 to 129 A/m, respectively. Thereafter, although the applied load increases significantly from 40 to 70 kN, both $\Delta H_{t,x}$ and $\Delta H_{n,z}$ decrease slightly from 117 to 48 A/m and from 77 to 28 A/m, respectively.

Figure 4 presents the variations of the $H_{t,x}$ and $H_{n,z}$ components along the scanning line loaded from 80 to 110 kN in the plastic stage. One may observe that the magnetic curves continue to evolve with slight alteration in terms of magnitude and shape. The maximum magnetic fields in the $H_{t,x}$ and $H_{n,z}$ curves decrease slightly from 449 to 397 A/m and 706 to 610 A/m, respectively. In addition, the adjacent weeny waveforms seem to disappear from the middle section of the magnetic curves.

Compared with the evolution of the magnetic curves measured from the left side of the scanning line, another interesting feature in Fig. 2 is that the magnetic traces on the right side demonstrate a more conspicuous change at various applied loads. Accordingly, curve *AB* and curve *CD* are intercepted from the entire $H_{t,x}$ and $H_{n,z}$ curves as shown in Fig. 2. The variations of the magnetic curves *AB* and *CD* with the increase of load are further presented in Fig. 5. One can see that the *AB* curves corresponding to the tangential component $H_{t,x}$ present good linearity along

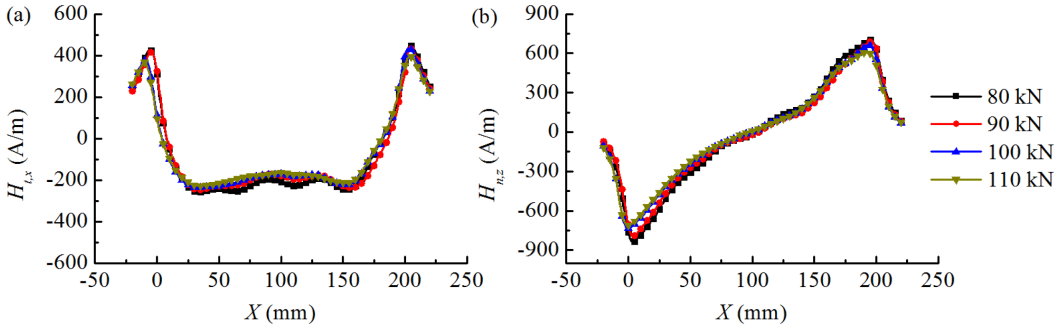

Fig. 4. (Color online) Variation of the RMF components with the increase of load in the plastic stage: (a) tangential component $H_{t,x}$; (b) normal component $H_{n,z}$.

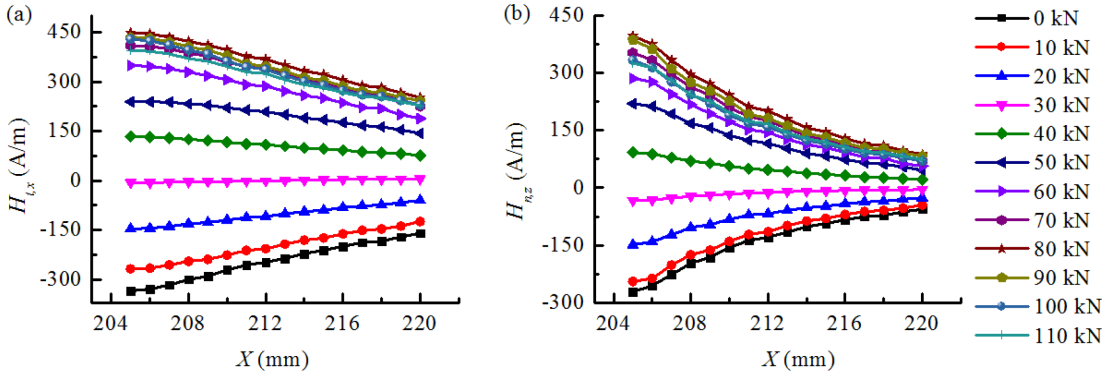

Fig. 5. (Color online) Variations of $H_{t,x}$ and $H_{n,z}$ at various applied loads in different deformation stages: (a) curve *AB*; (b) curve *CD*.

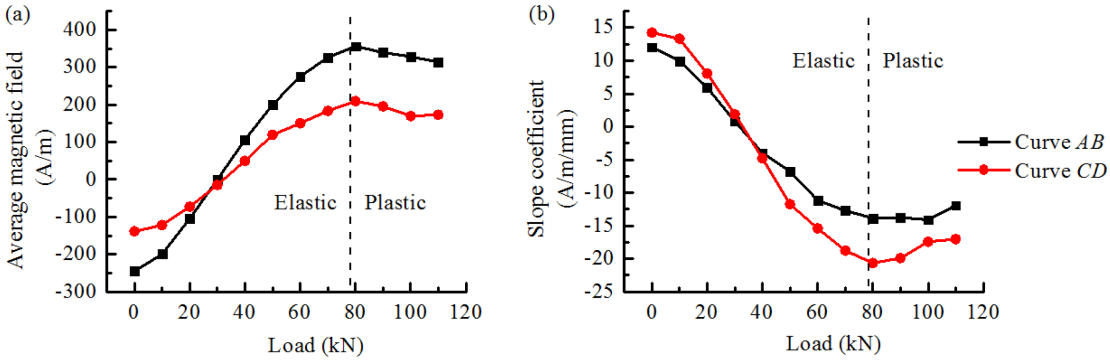

Fig. 6. (Color online) Variations of the average magnetic field and the slope coefficient of curves *AB* and *CD* at various applied loads in different deformation stages: (a) average magnetic field; (b) slope coefficient.

the scanning line, and the *CD* curves corresponding to the normal component $H_{n,z}$ are comprised of a series of oblique lines like a bellmouth. When the tensile load is below 80 kN, which is within the elastic stage, curve AB moves upward with an increase of the magnetic value. Similar results can also be observed in Fig. 5(b), but it seems that a different pattern emerges. Curve *CD* moves upward and rotates clockwise around the right edge of the scanning line. However, as the deformation proceeded into the plastic stage, curve *AB* starts to move downward with a slight decrease of the magnetic magnitude. Curve *CD* begins to rotate counterclockwise with a slight decrease of the slope.

Figure 6 shows the variations of the average magnetic field and the slope coefficient of curves *AB* and *CD* with the increase of load. One can observe that the variations of the average magnetic field and the slope of curve *AB* resemble that of curve *CD*. As shown in Fig. 6(a), the average magnetic field increases steadily in the elastic stage, and decreases slightly in the plastic stage. However, an opposite behavior can be observed in Fig. 6(b), the slope coefficient decreases drastically in the elastic stage, and increases slightly in the plastic stage. All of these results indicate that both the average magnetic field and the slope coefficient of curves *AB* and *CD* are effective in characterizing the elastic and plastic deformation stages. Additionally, during the elastic deformation stage, it seems that the applied load is highly related to the average magnetic field and the slope coefficient which provide a promising tool to analyze the stress in ferromagnetic materials. Previous studies also demonstrate that the slope coefficient of the magnetic curves can be utilized to characterize the deformation stages of steel specimens [5, 6, 12, 13]. However, the magnetic curves in their tensile tests were measured within the longitudinal axis of the specimens, and the specimens were preliminarily demagnetized. For an undemagnetized specimen, its initial remanences introduced by manufacturing process are non-uniformly distributed as shown in Fig. 2 at 0 kN. In the current study, it seems that an effective way for characterizing deformation stages is achieved which is to analyze the RMF signals outside the longitudinal axis of the specimen.

It can be observed from the preceding results that the magnetic fields emerge a gradual rate of change in the elastic stage and remain relatively stable in the plastic

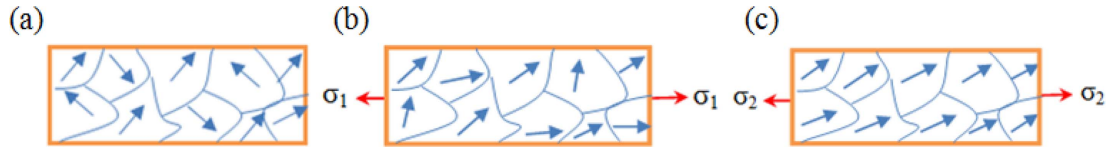

Fig. 7. (Color online) Schematic diagram of domain's reorientation induced by stress: (a) initialorientation of magnetic domains; (b) orientation of magnetic domains with increasing stress; (c) magnetic domains turning to the same ordering with further increase of stress.

stage. This is highly related to the stress and microstructural changes during the loading process. In the elastic stage, the application of load promotes the unpinning of domain walls and the rotation of magnetic moment towards the tensile direction [5, 6]. As the applied load increases, more magnetic domains are starting to rotate and the reorientation rate changes at a more gradual rate. In the plastic stage, the dislocations gradually pile up and interconnect as cell structures to form dislocation walls, which create some obstacles to the movement of magnetic domains. In addition, the residual compressive stress after unloading causes the magnetic moment reorient in perpendicular direction to the previous tensile direction. The balanced state could be obtained when all magnetic domains perform an entire rotation [9, 13, 16]. A schematic diagram is proposed to illustrate the magnetic domain's reorientation induced by the applied load [17]. As shown in Fig. 7(a), in the initial state, the orientations of the magnetic domains are in disorder. When the load is applied to the specimen, those magnetic domains whose orientation is near the load direction tend to rotate first toward the tensile direction as shown in Fig. 7(b). Then with the applied load increasing, the imperfection and residual stress in the specimen begin to adjust and more irregular magnetic domains are starting to rotate as well, and gradually turn to the same ordering as shown in Fig. 7(c). This leads to the observed stress-induced variations of the magnetic curves ($H_{t,x}$ and $H_{n,z}$) and the magnetic fluctuations ($\Delta H_{t,x}$ and $\Delta H_{n,z}$) in the region between two dashed lines.

However, the magnetic field changes at two ends of the specimen are much more complicated than that in the middle section. Three factors besides the action of load must be taken into consideration. Firstly, tensile testing machine fixture has a magnetic field itself under the long-term use, which inevitably influences the surface magnetic fields of the specimen. Secondly, after the specimen is clamped, the additional magnetic fields are induced in the two fixtures, since compressive stress is introduced [7]. The measured magnetic fields at both clamped ends are easily disturbed and affected. Finally, there is an abrupt decrease of permeability at two ends of the specimen since it has an air-gap in the area away from the specimen, which causes a sharp change in the magnetic property along the scanning line. All these factors induce the observed magnetic field changes and the generation of the abnormal magnetic peaks on either side of the specimen. Since the permeability and the magnetic charges at two ends of the specimen change concomitantly with the increase of load [18, 19], the abnormal magnetic peaks are becoming more prominent and finally tend to be stable on either side of the specimen. As a result, the initial load-free curve changes to the final stable curve with the applied load increasing. Interestingly, although the RMF signals at two ends of the specimen are influenced by a number of factors, the average magnetic field and the slope coefficient of curves *AB* and *CD* are still positively correlated with tensile load in the elastic stage and weakly correlated in the plastic stage, which suggest that the prevailing magnetization of the specimen presumably is the stress-induced magnetic field. Therefore, analyzing the RMF signals outside the longitudinal axis of the specimen makes it possible to characterize elastic-plastic deformation stages.

To further investigate the RMF distribution characteristics surrounding the specimen, the $H_{t,x}$ and $H_{t,y}$ components of 150 measurement points in the *XY* plane were recorded. Figure 8 shows the corresponding two-dimensional vector distribution of the RMF at several applied loads. It can be clearly seen that the specimen tends to be magnetized as a magnet with a north pole and south pole at two ends with the increase of load. With the applied loads of 0 kN and 10 kN (Fig. 8(a) and Fig. 8(b)), the arrows are in disordered directions and short length in the area away from the specimen. As the applied load is increased to 40 kN (Fig. 8(c)), the magnetic field distribution behaves to a first approximation like the magnetic field surrounding a simple bar magnet, which can be seen more clearly when the applied load is increased to 60 kN (Fig. 8(d)). Thereafter, the two-dimensional vector distribution of the RMF reverts to a more gradual rate of change in the plastic stage. With the applied loads of 80 kN and 100 kN (Fig. 8(e) and Fig. 8(f)), the magnetic vector distribution resembles each other with slight

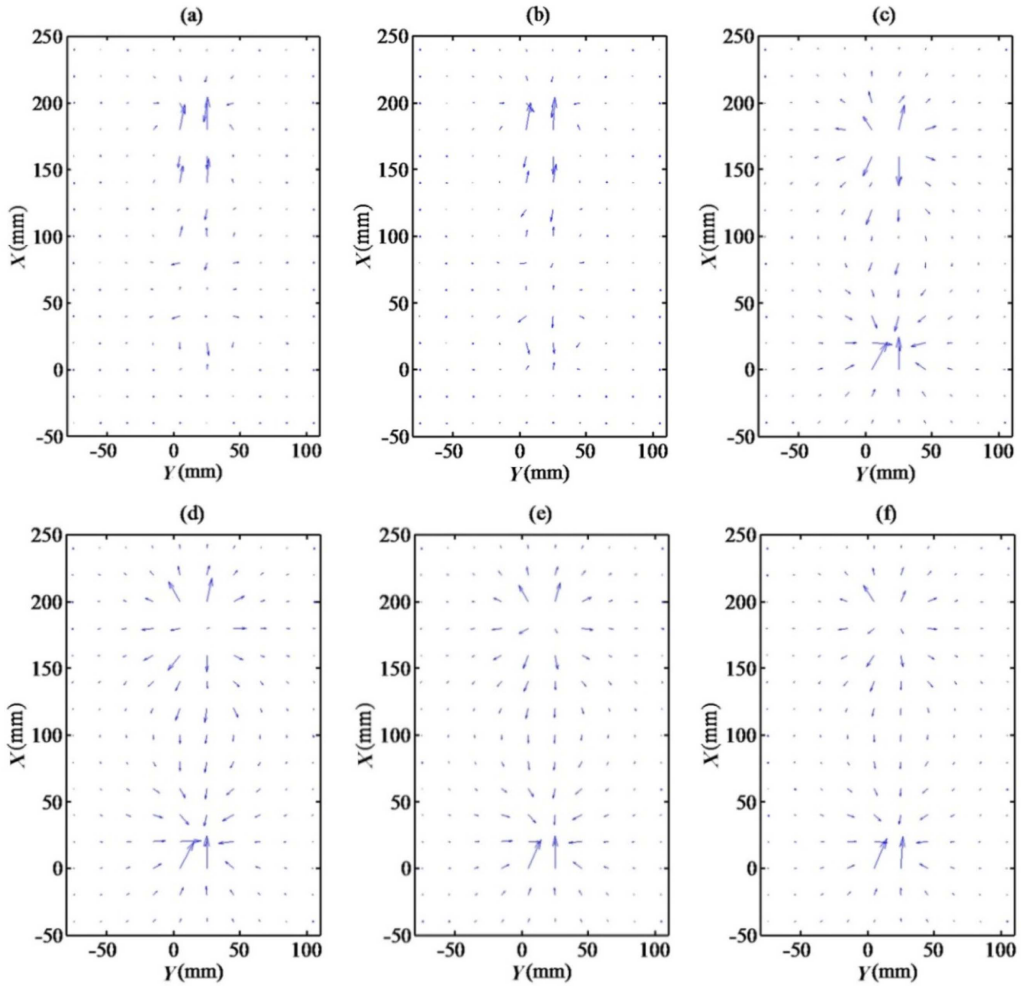

Fig. 8. (Color online) Two-dimensional vector distribution of the RMF at several applied loads: (a) 0 kN; (b) 10 kN; (c) 40 kN; (d) 60 kN; (e) 80 kN; (f) 100 kN

differences in terms of magnitude and direction, which are consistent with the observed results from Fig. 4.

4. Conclusions

In this research, tensile tests were carried out to investigate the RMF variations of U75V steel specimens under different load levels. The RMF distribution along the scanning line demonstrates different characteristics in the elastic as well as the plastic loading stages. In the elastic regime, the amplitude of magnetic field variation reduces with the increasing loads. In the plastic regime, the RMF curves continue to evolve with slight alteration in terms of magnitude and shape. The result of analyzing the RMF signals outside the longitudinal axis of the specimen turns out to be an effective way for characterizing deformation stages. The two-dimensional vector distribution of the RMF in the *XY* plane indicates that the specimen tends to be magnetized as a magnet with a north pole and south pole at two ends. The RMF surrounding a steel specimen demonstrates a pattern similar to that of a magnetic field surrounding a rectangular magnet.

Acknowledgments

This work was supported by the Fundamental Research Funds for the Central Universities (2017QNA4022), the Zhejiang Provincial Natural Science Foundation of China (LZ12E08003), the Interdisciplinary Research Fund for Young Scholars in Zhejiang University (JCZZ-2013018). Additionally, Meili Fu wants to thank Wenwen Zhao, a beautiful and lovely girl who has given him the inimitable care and support over the years.

References

[1] J. W. Wilson, G. Y. Tian, and S. Barrans, Sensors & Actuators A Physical **135**, 381 (2007).
[2] S. Bao, M. L. Fu, S. N. Hu, Y. B. Gu, and H. J. Lou, American Society of Mechanical Engineers **4**, V004T03A006 (2016).
[3] M. Roskosz and P. Gawrilenko, NDT & E International **41**, 570 (2008).
[4] S. Bao, M. L. Fu, H. J. Lou, and S. Z. Bai, J. Magn. Magn. Mater. **441**, 590 (2017).
[5] L. H. Dong, B. S. Xu, S. Y. Dong, L. Song, Q. Z. Chen, and D. Wang, NDT & E International **42**, 323 (2009).
[6] C. L. Shi, S. Y. Dong, B. S. Xu, and P. He, J. Magn. Magn. Mater. **322**, 413 (2010).
[7] J. C. Leng, M. Q. Xu, M. X. Xu, and J. Z. Zhang, NDT & E International **42**, 410 (2009).
[8] K. Yao, B. Deng, and Z. D. Wang, NDT & E International **47**, 7 (2012).
[9] L. H. Dong, B. S. Xu, S. Y. Dong, Q. Z. Chen, and D. Wang, NDT & E International **41**, 184 (2008).
[10] J. C. Leng, M. Q. Xu, G. Q. Zhou, and Z. M. Min, Ndt & E International **52**, 23 (2012).
[11] E. S. Gorkunov, Russian Journal of Nondestructive Testing **50**, 617 (2014).
[12] M. L. Fu, S. Bao, S. Z. Bai, Y. B. Gu, and S. N. Hu, Journal of Harbin Institute of Technology **49**, 178 (2017).
[13] M. L. Fu, S. Bao, Z. Y. Zhao, and Y. B. Gu, Insight **60**, 90 (2018).
[14] S. Bao, and D. Zhang, Insight **57**, 401 (2015).
[15] S. Bao, S. N. Hu, L. Lin, Y. B. Gu, and M. L. Fu, Insight **57**, 683 (2015).
[16] P. J. Guo, X. D. Chen, W. H. Guan, H. Y. Cheng, and H. Jiang, J. Magn. Magn. Mater. **323**, 2474 (2011).
[17] S. Bao, H. F. Lou, and S. F. Gong, Insight **56**, 252 (2014).
[18] L. H. Dong, B. S. Xu, S. Y. Dong, and Q. Z. Chen, Nondestructive Testing and Evaluation **25**, 145 (2010).
[19] J. Paľa, J. Bydžovský, and P. Švec, Journal of Electrical Engineering **55**, 38 (2004).